Article

Analysis of Characteristics of Low Voltage Circuit Breaker by External Magnetic Field

Young-Maan Cho [1] , Hyun-Jong Park [2], Jae-Jun Lee [3],* and Kun-A Lee [4],*

[1] Reliability Assessment Center, Hyundai Electric & Energy Systems Co., Ltd., 17-10 Mabuk-ro, 240 bean-gil, Giheung-gu, Yongin-si 16891, Korea
[2] Launcher Technology Development Division, Korea Aerospace Research Institute, Daejeon 34133, Korea
[3] Department of Electrical Engineering, Yuhan University, 590 Gyeongin-ro, Bucheon-si 14780, Korea
[4] School of Social Safety System Engineering and Research Center for Safety and Health, Hankyoung National University, 327 Chungang-ro, Anseong-si 17579, Korea
* Correspondence: jaejunlee@yuhan.ac.kr (J.-J.L.); kalee@hknu.ac.kr (K.-A.L.)

Abstract: Recently, as interest in eco-friendly distributed power has increased, studies on the improvement of the performance of breakers such as DC breakers and on the reliability of existing AC breakers have been actively conducted. To improve the performance and reliability of these breakers, this paper conducted the analysis of characteristics of a low voltage circuit breaker using an external magnetic field. In this experiment, before the current-zero point, the cut-off time to improve the breaker performance is shortened and after the current-zero point, re-ignition, which is associated with reliability, is suppressed. According to the experimental results, the short-circuit characteristics before current-zero show a significant difference of 0.13 ms in the t_{21} section, and the dielectric recovery strength after current-zero shows a 13.3% performance improvement in the latter half of the DRV (dielectric recovery voltage) V-t curve. This result has significant meaning because it can be easily improved under the control of the external magnetic field. Hence, it can be applied to the interruption performance improvement of breakers through detailed research in the future.

Keywords: molded case circuit breaker; dielectric recovery strength; external magnetic field; short-circuit characteristics

1. Introduction

Recently, as interest in eco-friendly distributed power using solar power, wind power, batteries, etc. has increased, the trend of product development and research is rapidly changing from the AC system to the DC system [1–3]. These changes in R&D trends are accelerating as each country's carbon-neutral policies and ESG (environmental, social and governance) management of companies. Particularly, in the case of DC distribution products where the electrical resistance is more fragile than that of the AC distribution products, it is necessary to interrupt the inflow of over-current more quickly. Therefore, various studies are being conducted to improve performance, such as introducing a new structure to improve the performance of existing breakers [4–12].

The circuit breaker basically consists of a trip unit that detects the inflow of over-current, a driving unit that separates electrodes that are conducted, and an arc extinguishing unit that directly removes the arc [13]. Even if the environment installed with the DC distribution system changes, these are essential components of the distribution circuit breaker with over-current protection. Therefore, in order to improve the performance of the circuit breaker, it is recommended that the above-mentioned three components (trip unit, driving unit, arc extinguishing unit) are improved.

Sang-Jae Choi et al. proposed the direct current fault current limitation and interruption process of hybrid DC circuit breaker by using double quench [14]. Yaqobi et al. studied a low-voltage solid-state circuit breaker for a DC micro-grid cluster using a bidirectional

insulated-gate bipolar transistor (IGBT) for rapid detecting the fault current. [15]. In our precious research, the dielectric recovery strength according to materials of the splitter plate was studied and it was confirmed that the thermal conductivity of the material had a dominant effect on initial dielectric recovery [16].

Currently, research on DC breakers is being conducted based on AC breakers. In the industry, AC breakers are also used as alternatives. In this paper, existing AC breakers are used for technical research applicable to DC breakers.

The blocking phase can be divided into before and after current-zero, as shown in Figure 1. First of all, before current-zero, the current limitation effect that limits over-current and the arc phenomenon that occurs between the operation of the moving electrode and a fixed electrode mainly. When the over-current inflows, the moving electrode of the circuit breaker begins to be separated from the fixed electrode and arc is generated between the electrodes. The generated arc is extended and moved toward the splitter plate by the pressure of the hot-gas generated by the arc and the arc runner. As opening of the moving electrode. After that, the arc that reaches the splitter plate is stretched, divided, and cooled to be extinguished, and at this time, current-zero is formed [17].
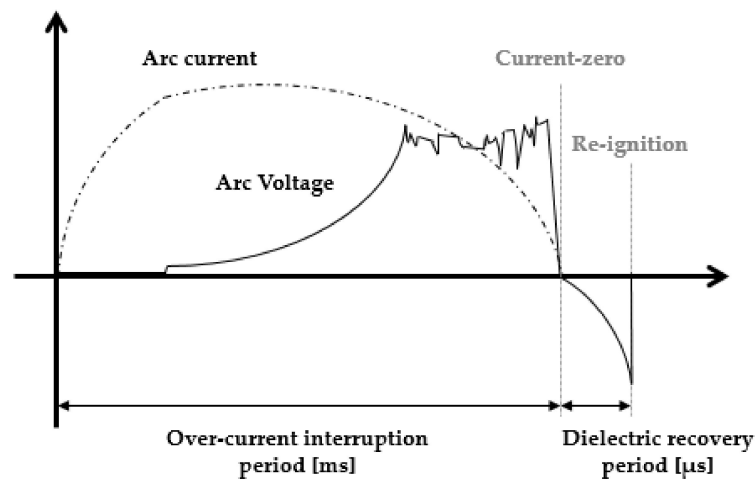

Figure 1. Classifications of phenomenon before and after the current-zero.

After current-zero, the re-ignition phenomenon occurs by hot gas. Hot gas generated by interruption is residual inside an arc extinguishing chamber, and this may decrease the dielectric strength between two open electrodes. Due to this reduced dielectric strength, arc is formed again between the two electrodes, and re-ignition occurs, resulting in a failure of interruption. To carry out the experiment, a structure is made for applying magnetic field to the circuit breaker. Using the structure, the effect of external magnetic field on the arc between electrodes are verified through finite element analysis (FEA) and pre-experiment. Through this process, the effect of the external magnetic field applied to a molded case circuit breaker (MCCB) on the short-circuit characteristics before the current-zero and the dielectric strength performance after the current-zero have been analyzed.

The composition of this paper is as follows. Section 2 deals with finite element analysis and experimental verification to analyze the effect of external magnetic fields on arcs formed between electrodes. In Section 3, short-circuit characteristics and dielectric recovery voltage are measured after being applied to the actual circuit breaker based on the previous verification. Finally, in Section 4, the effects of external magnetic fields are analyzed and conclusions were drawn based on the experimental results.

2. Analysis of the Effect of External Magnetic Field on Arc Current

2.1. Finite Elements Analysis

Finite element analysis is performed to confirm the effect of an external magnetic field on the arc current. The model for FEA is shown in Figure 2. The core is a laminated structure of a silicon steel sheet material. The coil wound around the core is an 18 AWG

enamel wire which has a diameter of 1.02 mm and an allowable current of 12 A. It consists of a total of three layers and 87 turns. The power source generating the arc current is equal to the positive half-cycle of 60 Hz sine wave and has a maximum value of 620 A. Through the model set in this way, it is confirmed how the force acting on the arc current changes according to the current of the coil. Figure 3 illustrates the distribution of magnetic flux density (B) when the arc current has a maximum value and when the current of 5 A flows in the coil. Since the core is not saturated by the coil current, the magnetic field is proportional to the current applied to the coil.
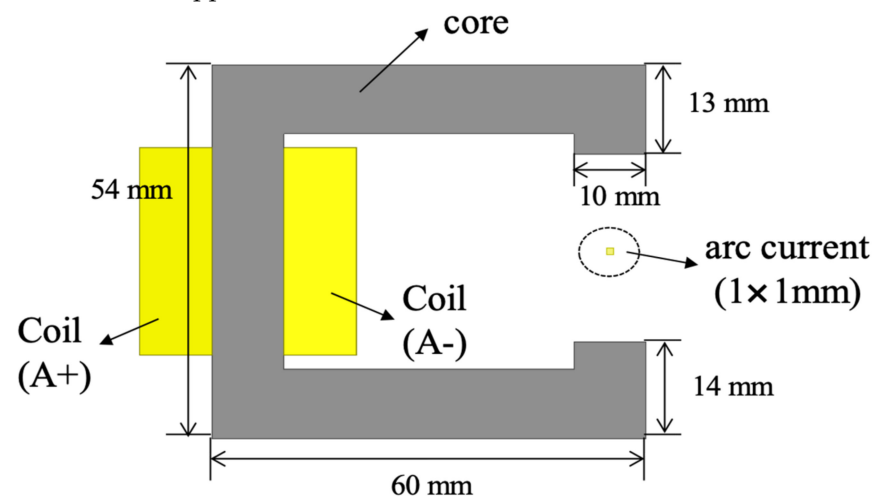

Figure 2. FEA model for verifying the effect of external magnetic field on arc current.
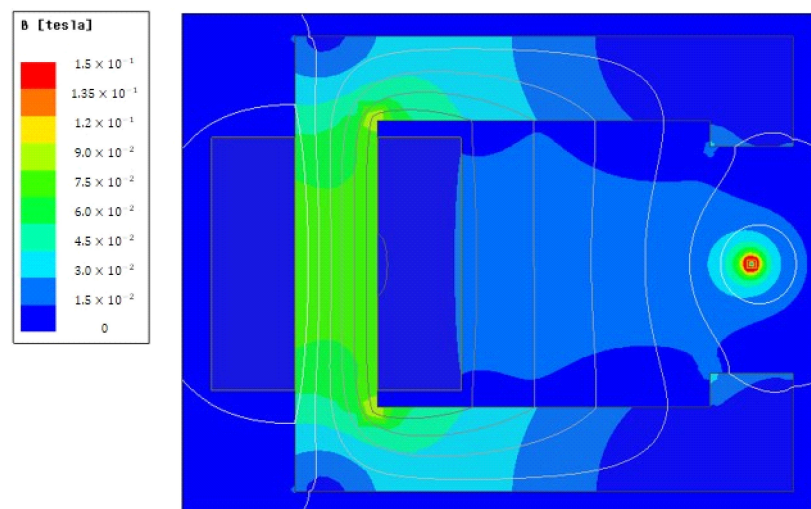

Figure 3. Magnetic density distribution when arc current is peak and coil current is 5 A.

Figure 4a shows the force acting on the arc current that depends on the magnitude of the current applied to the magnetic field. Each current applied to the external magnetic field is 0, 1, 3 and 5 A. Figure 4b is the result of integrating the force with respect to time. Figure 4a shows that a negative directional force is generated at 0 and 1 A, and a positive directional force is generated above 3 A. In Figure 4b, the force is integrated with respect to time, so the tendency of force is more pronounced. The arc current generates a force in the direction of minimizing the co-energy of the external magnetic field and the magnetic field by the arc current. Therefore, a negative force is generated even when no current is applied to the core, and a positive directional force acts when the intensity of the external magnetic field is greater than this force. The total force of the current applied to the coil is linearly proportional and the force varies from negative to positive at approximately 2.7 A.
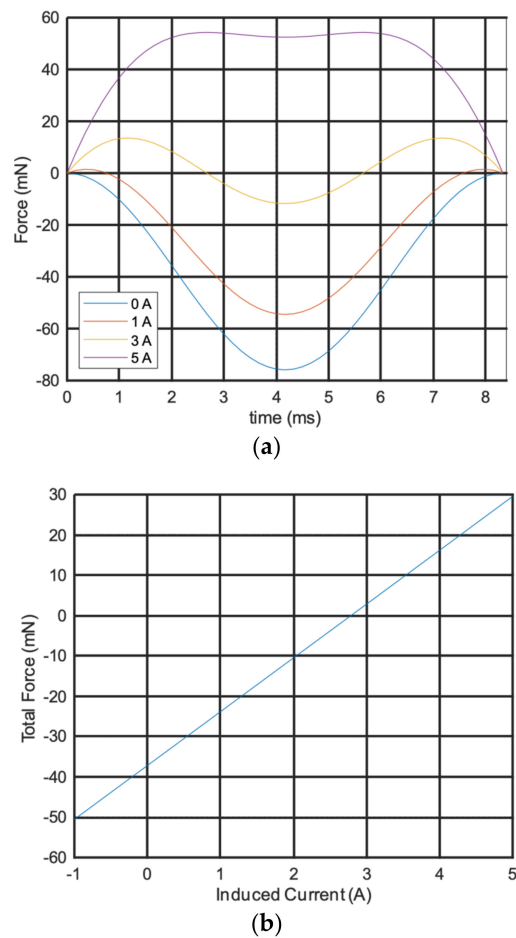
(a)

(b)

Figure 4. The Results of Finite Element Analysis. (**a**) Force on discharge current over time by external magnetic current; (**b**) Integration of the forces acting on the discharge current according to the external magnetic current.

2.2. Pre-Experiment

Based on the previous simulation results, a pre-experiment is performed as shown in Figure 5. The two electrodes are installed such that the distance between them is 27 mm, and DC current is applied to the coil of the core.
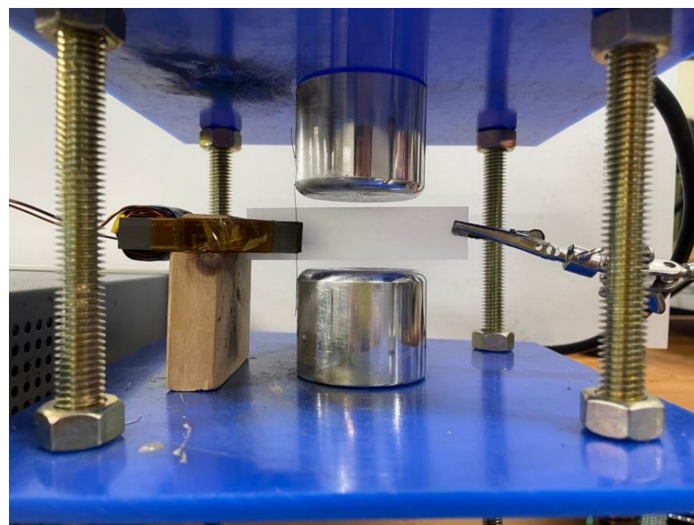

Figure 5. The test set-up of pre electrode experiment.

A thin wire is connected between the separated electrodes, and an over-current flows through this thin wire. The arc generated by the burning of this wire becomes longer, and the separation of the fixed electrode and the moving electrode is substituted.

The conditions of the experiment are when DC 1, 3, and 5 A are applied to the enamel line wound around the core and when there is no magnetic field. The effect on the arc generated between the electrodes is examined under these conditions. In order to measure the movement of the arc and the effect of the magnetic field, a parchment paper is located at the place where the arc current is generated. In this paper, an experiment is performed in a low magnetic field to investigate the tendency of an external magnetic field to affect MCCB performance.

As illustrated in Figure 6, the experiment results show that as the applied magnetic field increases, the effect on the magnetic field formed between the electrodes increases. In the figure, the black line represents the position of the wire connected between the electrodes, and the Lorentz force by the external magnetic field is generated to the right. Figure 6a,b show the case of no external magnetic field and the inflow of 1 A, respectively, and show that an arc occurs on the left side of the wire This corresponds to the negative force acting at a current of 2.7 A or less, as seen in the previous FEA results. In contrast to the case of no magnetic field, in the case of 1 A inflow, the paper is widely blacked due to the influence of the external magnetic field and the magnetic field due to over-current. Figure 6c is the case of 3 A inflow, and unlike the previous result, the paper is blackened on the slightly right side. This is because it is similar to 2.7 A in that the force changes from negative to positive. Finally, Figure 6d illustrates the case of 5 A inflow, and it is confirmed that the location of the arc is significantly formed on the right side of the wire. In addition, it can be seen that the lower part of the arc is more affected than the upper part, so the soot is formed farther away.
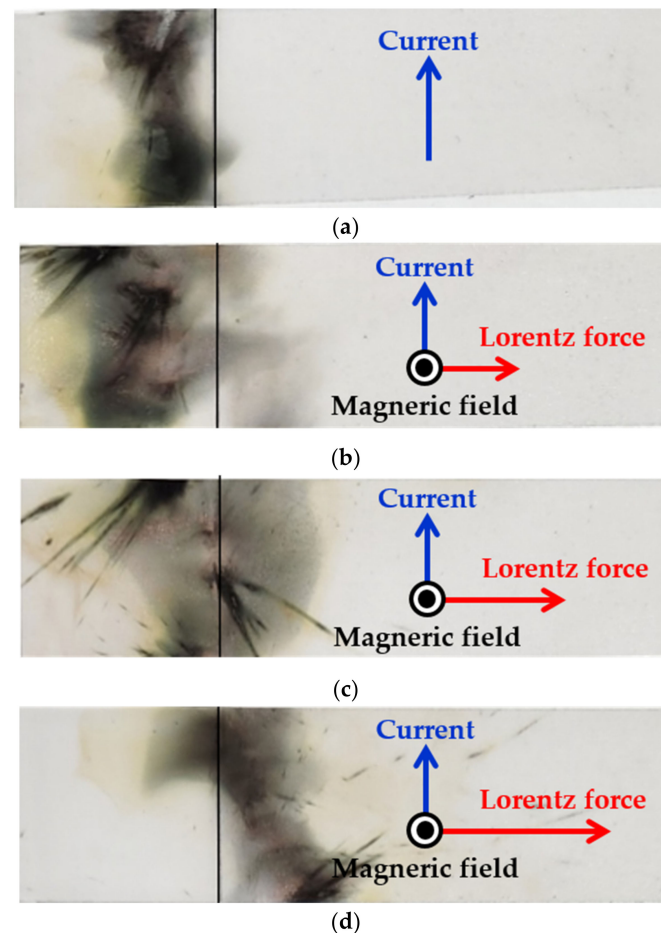

(a)

(b)

(c)

(d)

Figure 6. The Movements of Arc depending on External Magnetic Field. (**a**) without Magnetic field; (**b**) with Magnetic field (I = 1 A); (**c**) with Magnetic field (I = 3 A); (**d**) with Magnetic field (I = 5 A).

3. Experimental Studies According to External Magnetic Field

3.1. Experimental Set-Ups

The circuit used in the experiment is shown in Figure 7. The charged capacitor C_S generates an over-current and the frequency is adjusted through L. The frequency used in the experiment is 60 Hz, which is the commercial frequency. Thereafter, an over-current flows to the circuit breaker by applying a gate signal to the thyristor. A capacitor C_0 connected in parallel to a circuit breaker was installed to model the recovery voltage of the system applied to the circuit breaker after current zero. By adjusting the capacitance of C_0, re-ignition for measuring the dielectric recovery voltage between electrodes after current zero can be arbitrarily generated [13]. The capacitor C_S is charged with 600 V, and the over-current flowing into the breaker is 2.5 kA. All experiments are performed in a laboratory maintaining the conditions of temperature 20~25 °C and humidity 45~55 %R.H using an air conditioner in order to exclude the effect of environmental conditions.
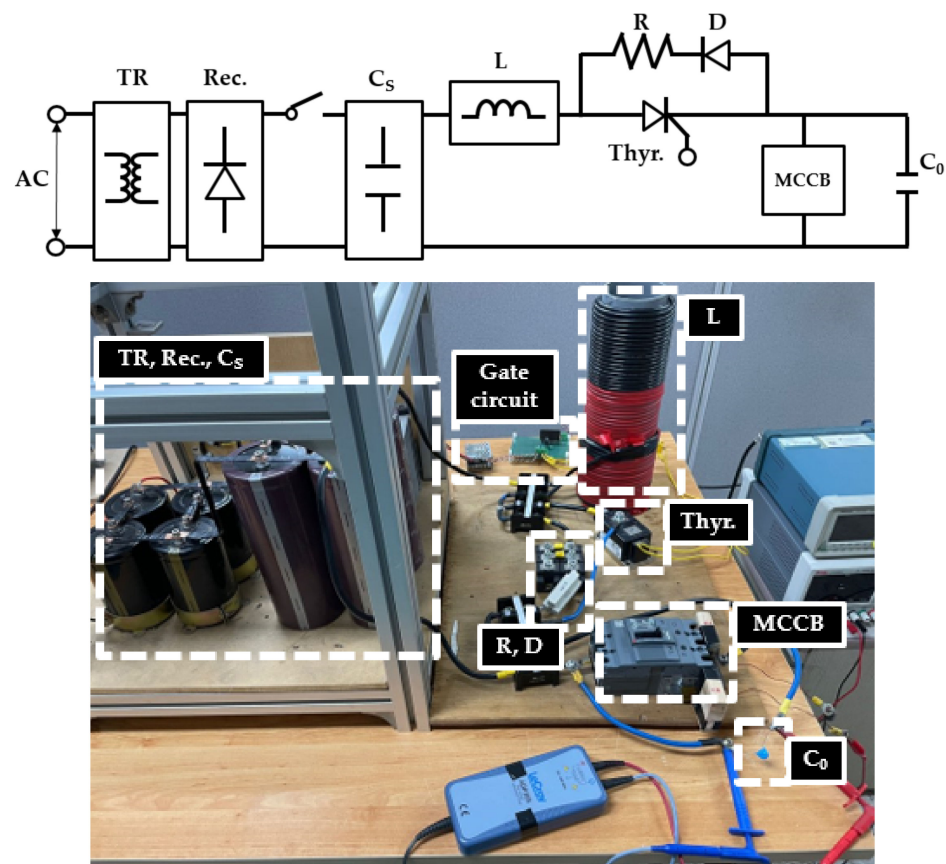

Figure 7. The test circuit and set-up.

3.2. Short-Circuit Characteristics

In order to analyze the short-circuit characteristics of the circuit breaker by an external magnetic field, the measurement period is determined from a representative waveform. Figure 8 shows for these periods.

Here, t_{10} is the section where an over-current flows into the breaker and the moving electrode starts to be separated from the fixed electrode due to the Lorentz force between the electrodes. t_{21} is a section where, after two electrodes are separated, the moving electrode is opened, and the arc generated between the electrodes moves to the splitter plate. A t_{32} is a section in which arc energy is consumed after reaching the splitter plate. As a circuit breaker, Schneider's EZC100H model is used in the experiment. To apply an external magnetic field to the arc generated between two electrodes, the core used in the pre-experiment is installed the circuit breaker, as shown in Figure 9.
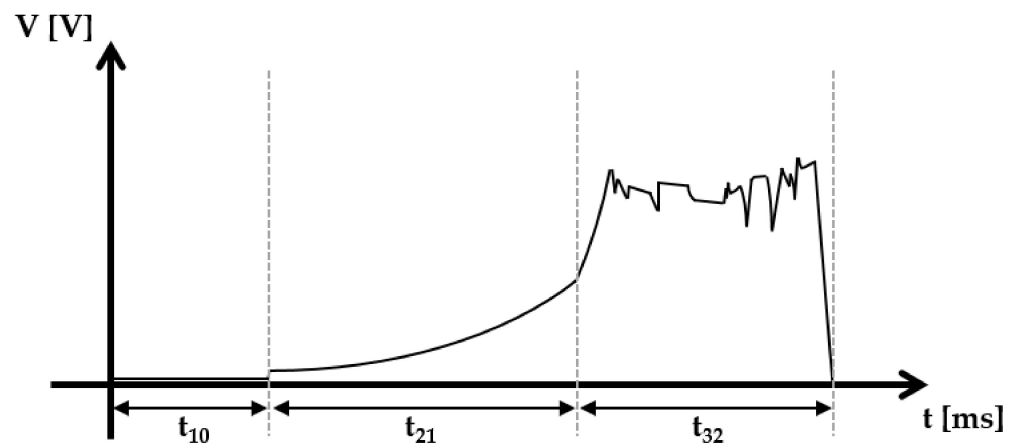
Figure 8. The measurement section for analysis of short-circuit characteristics.

Figure 9. Structure for applying external magnetic field and the circuit breaker.

The conditions of each experiment are as follows:

(1)   When there is no external magnetic field (I = 0 A);
(2)   When external magnetic field is applied (I = 5 A).

Table 1 shows each repeated experimental values and arithmetic mean values.

Table 1. Short-circuit characteristics Experimental results.

Case without an External Magnetic Field (I = 0 A)							[ms]
Experiment Number	**1**	**2**	**3**	**4**	**5**	**6**	**AVG.**
t_{10}	2.41	2.84	2.61	2.20	2.86	2.21	2.52
t_{21}	4.62	4.29	4.62	4.83	4.26	5.01	4.61
t_{32}	1.45	1.32	1.28	1.39	1.46	1.35	1.37
Case with an External Magnetic Field (I = 5 A)							**[ms]**
Experiment Number	**1**	**2**	**3**	**4**	**5**	**6**	**AVG.**
t_{10}	2.47	1.99	1.79	3.10	3.89	2.00	2.54
t_{21}	4.61	5.14	5.24	3.95	2.94	5.01	4.48
t_{32}	1.27	1.31	1.38	1.38	1.52	1.45	1.38

Figure 10 shows the resulting waveform of no external magnetic field, and Figure 11 shows the waveform when the external magnetic field is applied.
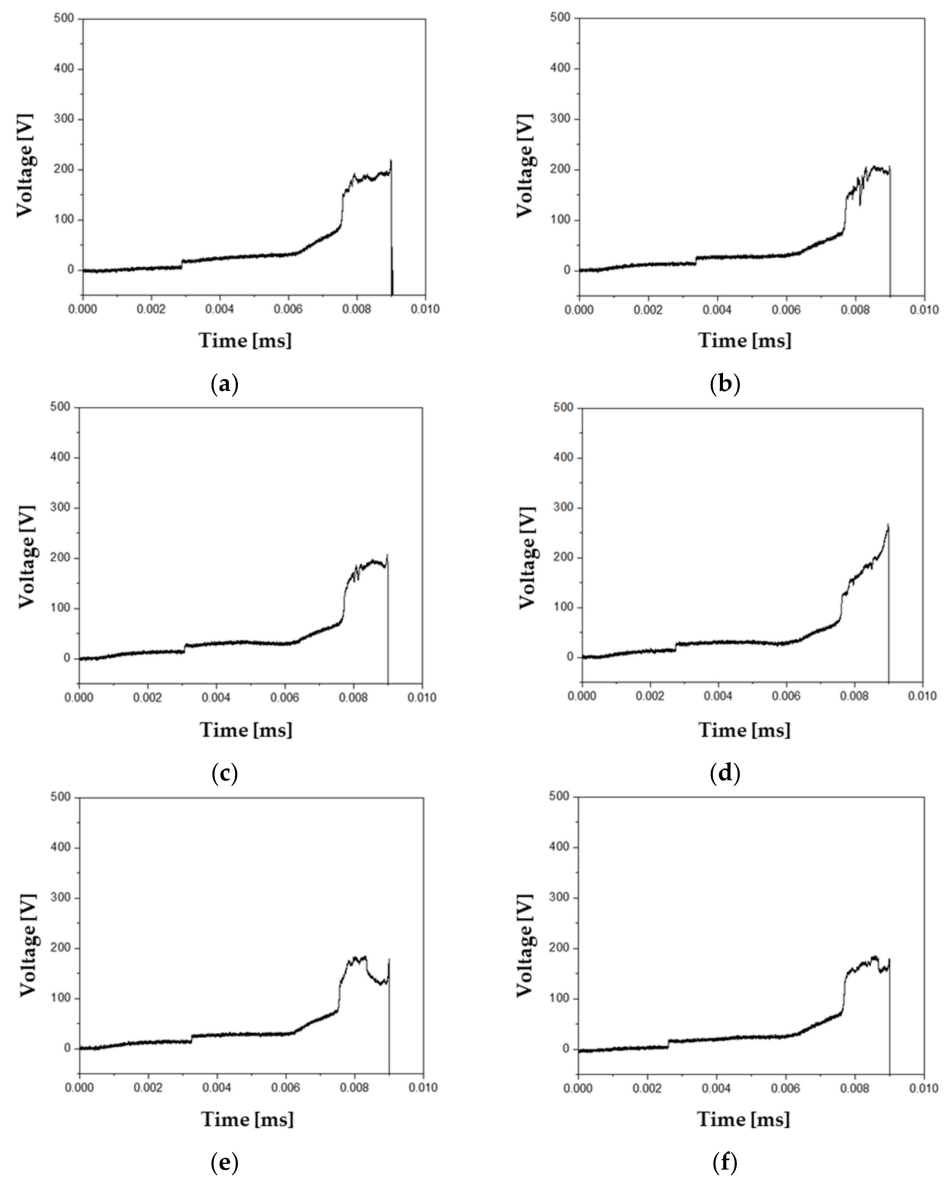

Figure 10. The waveform when there is no external magnetic field (I = 0 A). (**a**) No.1; (**b**) No.2; (**c**) No.3; (**d**) No.4; (**e**) No.5; (**f**) No.6.

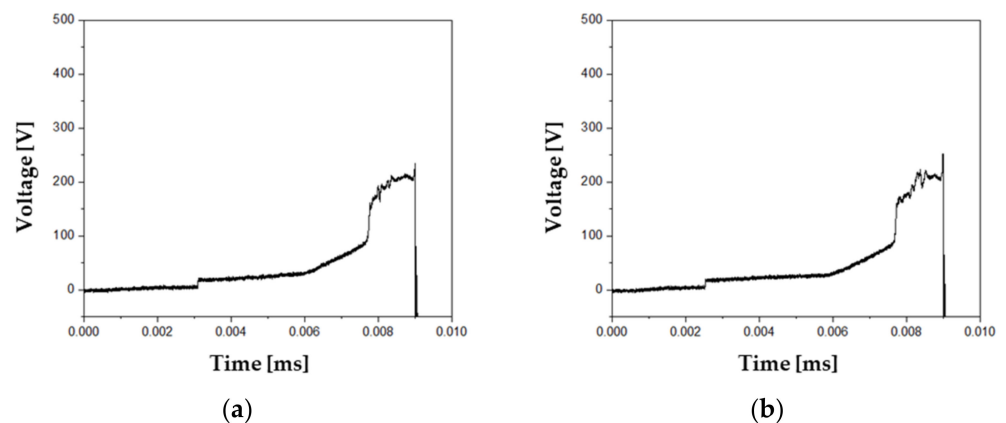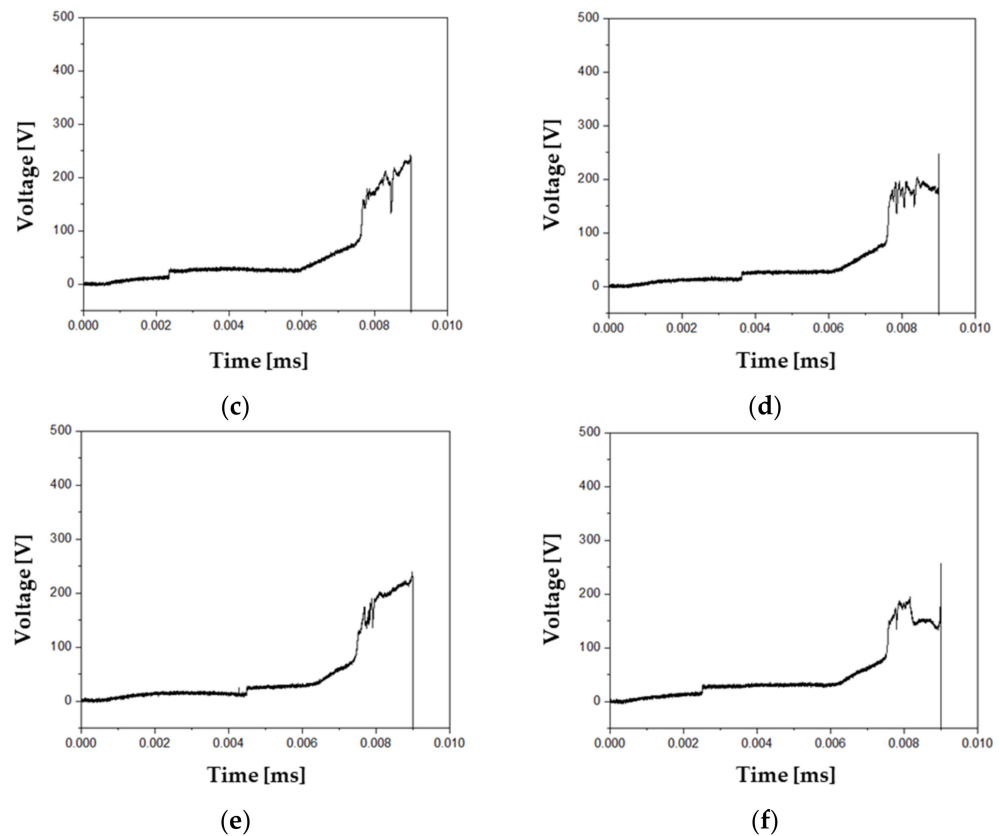**Figure 11.** *Cont.*

Figure 11. The waveform when the external magnetic field is applied. (I = 5 A). (**a**) No.1; (**b**) No.2; (**c**) No.3; (**d**) No.4; (**e**) No.5; (**f**) No.6.

The results are as follows. First, in t_{10} period, there is little difference in the presence or absence of a magnetic field of about +0.02 ms. This means that the external magnetic field does not affect the internal Lorentz force determining t_{10}. This internal Lorentz force is generated when the over-current flowing into the fixed electrode reciprocates, and in order to generate a large Lorentz force, the interval between the paths through which the current reciprocates should be narrow. Applying this experiment, in order for the external magnetic field to affect the Lorentz force, many magnetic fields must pass due to the wide gap in the passage, but it is difficult to have a significant impact because the gap in this passage must be small.

In addition, the generation position of the external magnetic field is not a fixed electrode with a gap in the path but occurs between the fixed electrode and the movable electrode, so it is judged to have an insignificant effect.

In t_{21} period, there is significant difference of -0.13 ms. The arc current moves fast by receiving a force in the direction of the splitter plate by an external magnetic field. It is faster than the case of no external magnetic field. From the experimental results, it can be seen that the sum of t_{10} and t_{21} has a relatively constant value regardless of the deviation. It is about 7.1 ms for the case without external field and 7.0 ms for the case with external field. The difference above is a significant difference in that this sum is a value that is difficult to replace with another factor. Time reduction at t_{21} is important to relate to the extinguish time of the arc current afterwards. This time can be adjusted by the external magnetic field.

Even in the t_{32} period, there is a small difference of 0.01 ms. Factors influencing t_{32} include the size and number of splitter plates, the value and temperature of arc current, and the temperature of external air, but there is no significant influence on this.

3.3. Dielectric Recovery Strength Performance

The dielectric recovery voltage after current-zero is measured by repeatedly performing an experiment that intentionally generates re-ignition through adjusting the C_0 value. Figure 12 shows a schematic diagram of the re-ignition that occurs after current-zero. When re-ignition occurs, the waveform of the arc voltage shows a form in which the dielectric breakdown occurs and the arc current is re-formed.
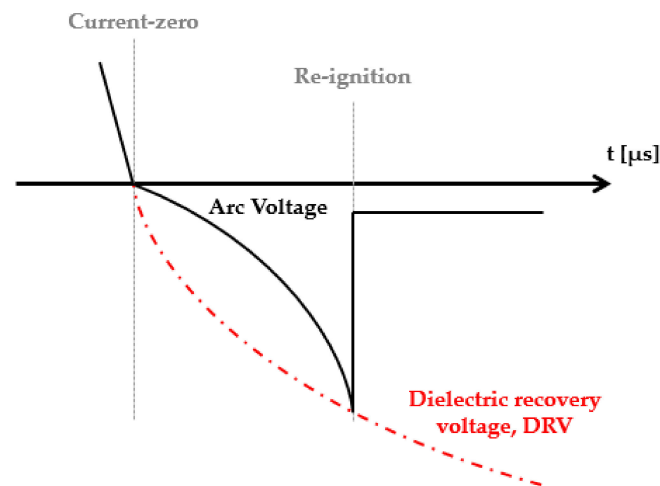

Figure 12. A schematic diagram of the re-ignition.

In order to measure the dielectric recovery voltage between electrodes, the time and voltage of the position where the re-ignition occurs are measured three times each to derive an arithmetic average value. At this time, the C_0 capacities are 0.47 μF, 1 μF, and 10 μF, respectively, and are related to the time when re-ignition occurs. The experimental waveform according to each C_0 capacitance is shown in Figures 13 and 14.
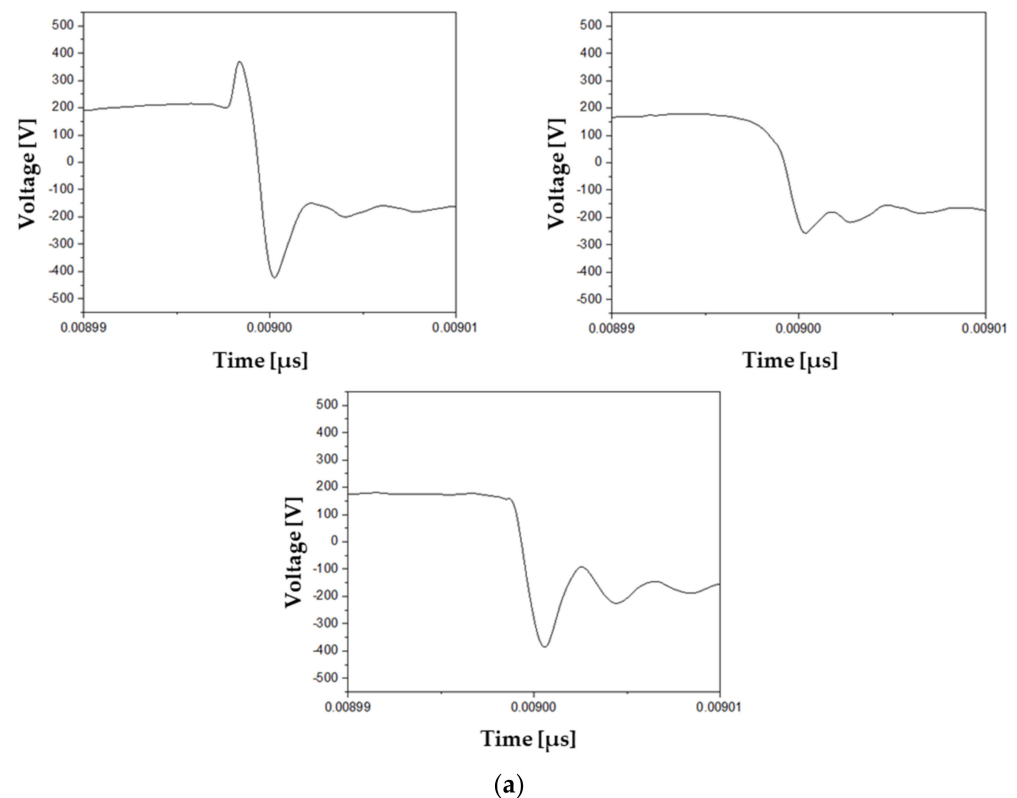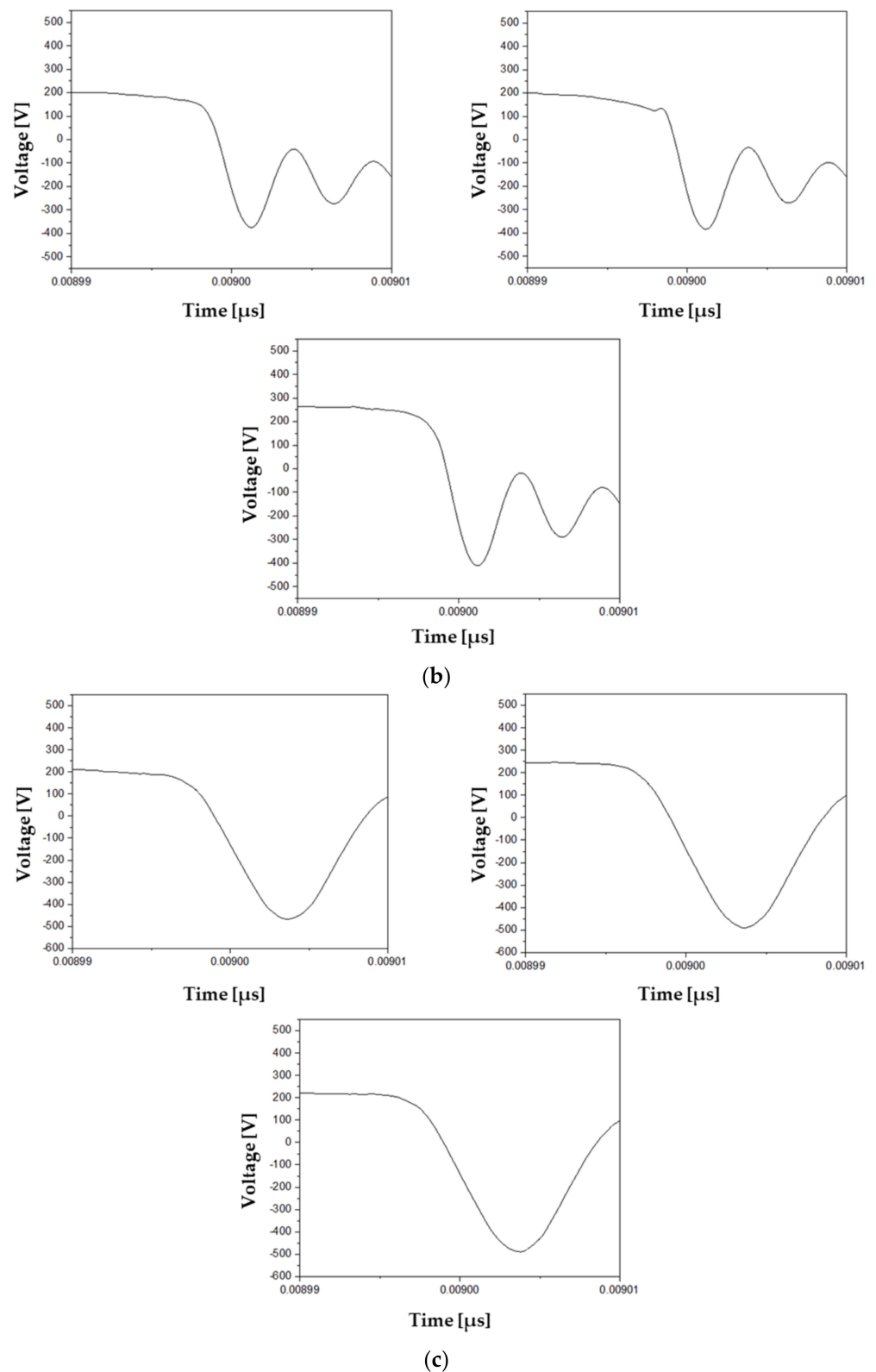

(a)

Figure 13. *Cont.*

Figure 13. Experimental Waveforms of dielectric recovery performance without an external magnetic field (I = 0 A). (**a**) C_0 = 0.47 µF; (**b**) C_0 = 1 µF; (**c**) C_0 = 10 µF.

Table 2 shows the DRV (dielectric recovery voltage) without an external magnetic field (I = 0 A) and with an external magnetic field (I = 5 A). Each C_0 value (0.47, 1, 10 µF) shows the average voltage and average time. Using this voltage and time values, Figure 15

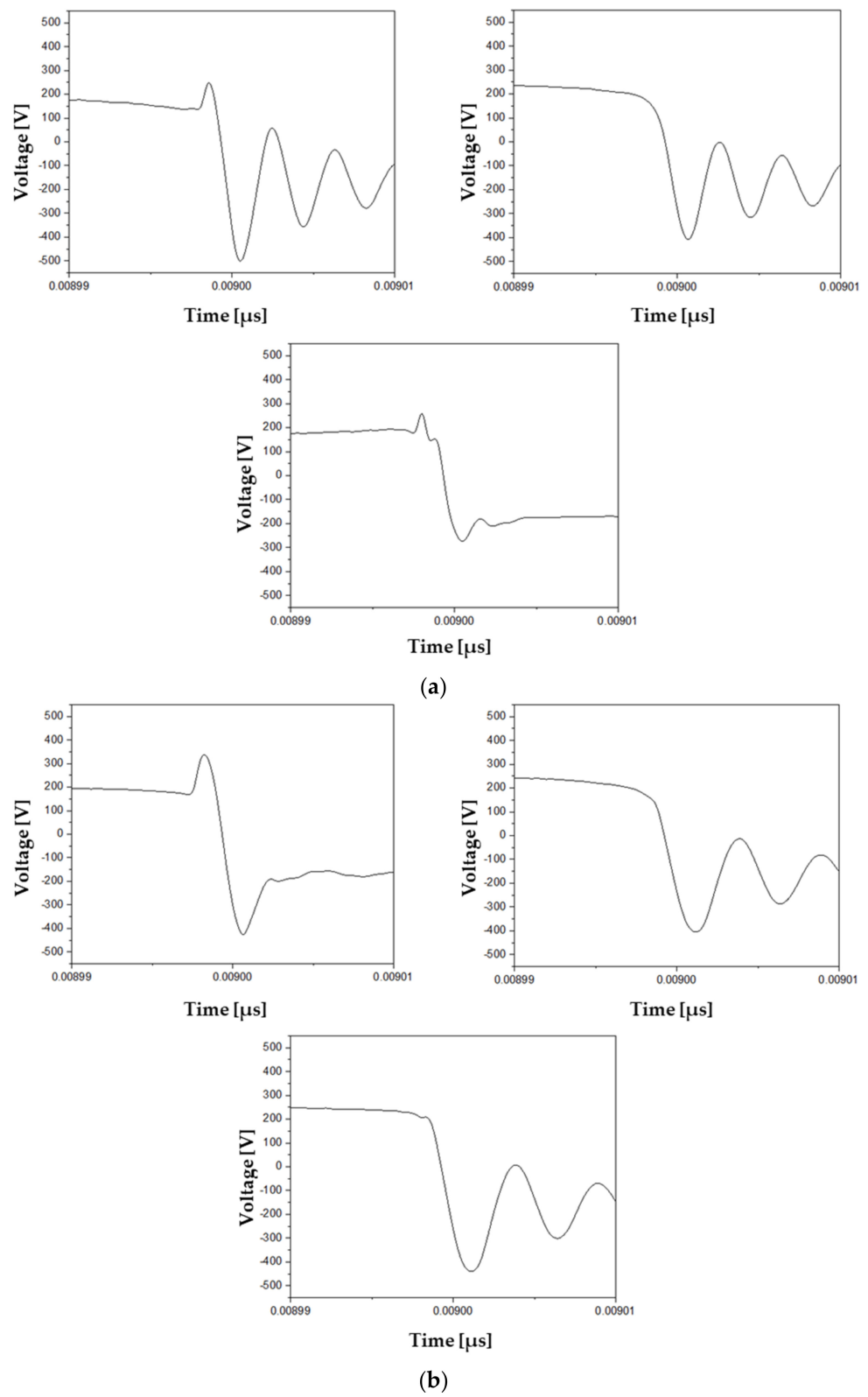shows the V-t curve of the DRV without external magnetic field (I = 0 A) and with external magnetic field (I = 5 A)
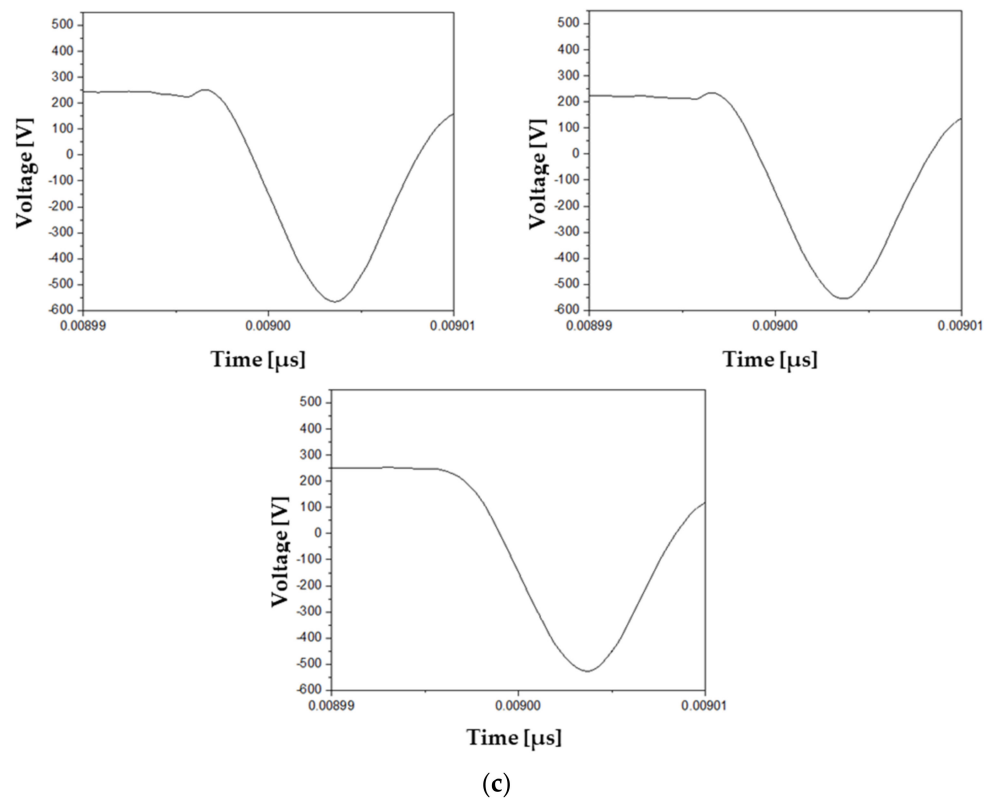

(a)

(b)

Figure 14. *Cont.*

(**c**)

Figure 14. Experimental Waveforms of dielectric recovery performance with an external magnetic field (I = 5 A). (**a**) C_0 = 0.47 µF; (**b**) C_0 = 1 µF; (**c**) C_0 = 10 µF.

Table 2. Measurement results of dielectric recovery voltage.

Category	C_0 [µF]	Voltage [V]	Time [µs]	Average Voltage [V]	Average Time [µs]
DRV without an external magnetic field (I = 0 A)	0.47	386 258 423	0.96 1.13 1.23	355.67	1.11
	1	375 384 411	1.90 2.05 2.02	390.00	1.99
	10	467 491 489	4.37 4.53 4.63	482.33	4.51
DRV with an external magnetic field (I = 5 A)	0.47	501 408 275	1.23 1.31 1.23	394.67	1.26
	1	426 405 440	1.29 1.85 1.88	423.67	1.67
	10	557 555 527	4.09 4.64 4.76	546.33	4.50

DRV characteristics can be largely divided into initial state and latter state. The initial state is affected by the cooling performance of the splitter plate, and the latter state is affected by the emission of hot gas generated by arc extinguishing, etc. The results of this paper are as follows. The differences in dielectric recovery voltages corresponding to C_0

values (0.47 μF, 1 μF, 10 μF) are 39.0 V, 33.7 V, and 64.0 V, respectively. It is difficult to accurately compare the voltage values (y-axis) because the average time of each state is slightly different. However, the values of the initial state and the latter state are about twice different. This is interpreted in that the ionized hot gas generated in the process of extinguishing the arc receives a force from an external magnetic field in the direction of the exhaust port.
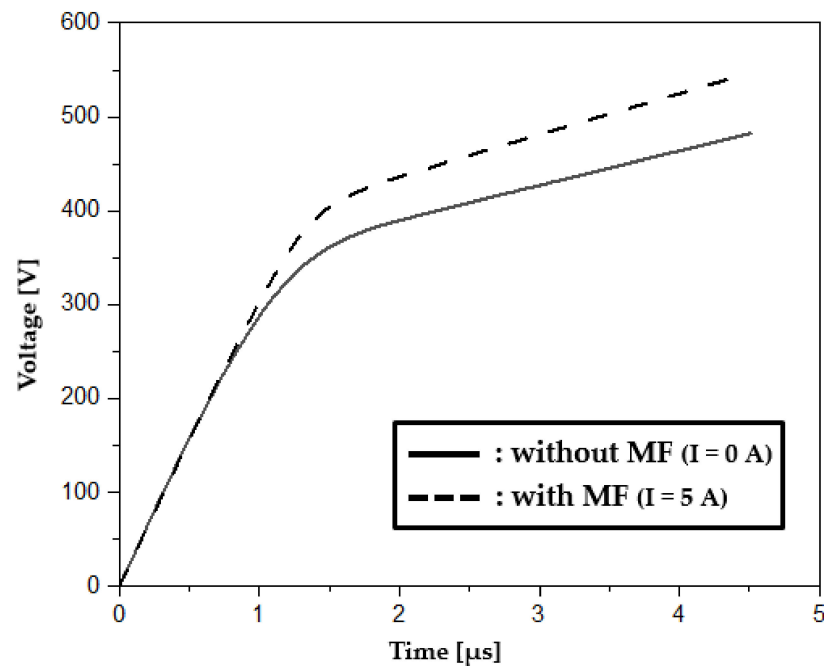

Figure 15. DRV V-t curve with or without an external magnetic field.

4. Conclusions

In this paper, the analysis of characteristics of low-voltage circuit breaker by the external magnetic field is performed. First, the FEA and the pre-experiment were performed to confirm the movement of the arc current by the magnetic field. In this experimental condition, the force acted in the targeted direction when 2.7 A, and its distribution was determined. Based on this, the performance of the low voltage circuit breaker for external magnetic fields was investigated through two experiments. These assessed short circuit characteristics before current-zero and dielectric recovery strength afterwards. In terms of short-circuit characteristics, it shows a significant decrease in t_{21} period in which the arc current generated between the fixed and moving electrodes moves to the splitter plate. This reduces the overall cutoff time and helps to improve reliability in that it secures a t_{32} time when the arc current is extinguished. In terms of dielectric recovery strength, there is an improvement of 13.3% in the latter state of the DRV V-t curve. Since the initial state performance can be improved by changing the material of the splitter plate, increasing the surface area, and decreasing a temperature decrease, the result can be applied in more various ways. This study confirms the improvement of the interruption performance before and after current-zero due to the presence or absence of an external magnetic field. Therefore, it is judged that the external magnetic field can be utilized when additional performance improvement is required depending on the environment or surrounding environmental conditions. For example, by adding a high-end product lineup with a built-in generator or devising a form that attaches to an existing circuit breaker in a modular way, it is expected to be possible to generate additional income and gain competitiveness in business. Additional research on the control of external magnetic fields is required in the future. In addition, if time control and spatial control are performed, it can help to improve the breaker's interruption performance.

References

1. Prabhala, V.A.; Baddipadiga, B.P.; Fajri, P.; Ferdowsi, M. An overview of direct current distribution system architectures & benefits. *Energies* **2018**, *11*, 2463.
2. Iweh, C.D.; Gyamfi, S.; Tanyi, E.; Effah-Donyina, E. Distributed Generation and Renewable Energy Integration into the Grid: Prerequisites, Push Factors, Practical Options, Issues and Merits. *Energies* **2021**, *14*, 5375. [CrossRef]
3. Gelani, H.E.; Dastgeer, F.; Nasir, M.; Khan, S.; Guerrero, J.M. AC vs. DC distribution efficiency: Are we on the right path? *Energies* **2021**, *14*, 4039. [CrossRef]
4. Fu, R.; Bhatta, S.; Keller, J.M.; Zhang, Y. Assessment of Cable Length Limit for Effective Protection by Z-Source Circuit Breakers in DC Power Networks. *Electronics* **2021**, *10*, 183. [CrossRef]
5. Ahmad, M.; Wang, Z. A Hybrid DC Circuit Breaker with Fault-Current-Limiting Capability for VSC-HVDC Transmission System. *Energies* **2019**, *12*, 2388. [CrossRef]
6. Kim, J.-Y.; Kim, H.-S.; Baek, J.-W.; Jeong, D.-K. Analysis of Effective Three-Level Neutral Point Clamped Converter System for the Bipolar LVDC Distribution. *Electronics* **2019**, *8*, 691. [CrossRef]
7. He, J.; Wang, K.; Li, J. Numerical Study on Multiple Arcs in a Pyro-Breaker Based on the Black-Box Arc Model. *Electronics* **2022**, *11*, 1702. [CrossRef]
8. Kim, W.; Kim, Y.-J.; Kim, H. Arc Voltage and Current Characteristics in Low-Voltage Direct Current. *Energies* **2018**, *11*, 2511. [CrossRef]
9. Parmar, D.; Gojiya, M. Analysis and improvement in repulsive force of 630 A frame Moulded Case Circuit Breaker (MCCB). *Int. Perspect Sci.* **2016**, *8*, 424–427. [CrossRef]
10. Wang, L.; Feng, B.; Wang, Y.; Wu, T. Bidirectional Short-Circuit Current Blocker for DC Microgrid Based on Solid-State Circuit Breaker. *Electronics* **2020**, *9*, 306. [CrossRef]
11. Tapia, L.; Baraia-Etxaburu, I.; Valera, J.J. Design of a Solid-State Circuit Breaker for a DC Grid-Based Vessel Power System. *Electronics* **2019**, *8*, 953. [CrossRef]
12. Wang, D.; Liao, M.; Wang, R.; Li, T.; Qiu, J.; Li, J.; Duan, X.; Zou, J. Research on Vacuum Arc Commutation Characteristics of a Natural-Commutate Hybrid DC Circuit Breaker. *Energies* **2020**, *13*, 4823. [CrossRef]
13. Cho, Y.-M.; Rhee, J.-H.; Baek, J.-E.; Ko, K.-C. Implementing a Dielectric Recovery Strength Measuring System for Molded Case Circuit Breakers. *Int. J. Electr. Eng. Technol.* **2018**, *13*, 1751–1757.
14. Choi, S.J.; Lee, J.H.; Lee, J.W.; Lim, S.H. Improvement of DC Fault Current Limiting and Interrupting Operation of Hybrid DC Circuit Breaker Using Double Quench. *Energies* **2021**, *14*, 4157. [CrossRef]
15. Yaqobi, M.A.; Matayoshi, H.; Danish, M.S.S.; Lotfy, M.E.; Howlader, A.M. Low-voltage solid-state DC breaker for fault protection applications in isolated DC microgrid cluster. *Appl. Sci.* **2019**, *9*, 723. [CrossRef]
16. Cho, Y.M.; Lee, K.A. Experimental Study on Splitter Plate for Improving the Dielectric Recovery Strength of Low-Voltage Circuit Breaker. *Electronics* **2020**, *9*, 2148. [CrossRef]
17. Lee, K.A.; Cho, Y.M.; Lee, H.J. Circuit model and analysis of molded case circuit breaker interruption phenomenon. *Electronics* **2020**, *9*, 2047. [CrossRef]